Photoelectron spectra of hydrated electron clusters: Fitting line shapes and grouping isomers

James V. Coe[a)]
Department of Chemistry, The Ohio State University, Columbus, Ohio 43210

Susan T. Arnold, Joseph G. Eaton, Gang Ho Lee, and Kit H. Bowen[b)]
Department of Chemistry, Johns Hopkins University, Baltimore, Maryland 21218

(Received 17 December 2004; accepted 16 May 2006; published online 6 July 2006)

The photoelectron spectra of $(H_2O)^-_{n=2-69}$ and $(D_2O)^-_{n=2-23}$ are presented, and their spectral line shapes are analyzed in detail. This analysis revealed the presence of three different groupings of species, each of which are seen over the range, $n=11-16$. These three groups are designated as dipole boundlike states, seen from $n=2-16$, intermediate states, found from $n=6-16$, and bulk embryonts, starting at $n=11$ and continuing up through the largest sizes studied. Almost two decades ago [J. V. Coe *et al.*, J. Chem. Phys. **92**, 3980 (1990)], before the present comprehensive analysis, we concluded that the latter category of species were embryonic hydrated electrons with internalizing excess electrons (thus the term embryonts). Recent experiments with colder expansion (high stagnation chamber pressures) conditions by Neumark and coworkers [J. R. R. Verlet *et al.*, Science **307**, 93 (2005)] have also found three groups of isomers including the long-sought-after surface states of large water cluster anions. This work confirms that the species here designated as embryonts are in the process of internalizing the excess electron states as the cluster size increases (for $n \geqslant 11$). © *2006 American Institute of Physics*. [DOI: 10.1063/1.2212415]

INTRODUCTION

The collective interactions of water molecules are important in solvating an electron in bulk water, as is implied by the observation that an isolated water molecule will not attach an electron.[1,2] Due to such interactions, there is an enormous reduction in the photon energy required [6.5 eV (Ref. 3) and 6.4 eV (Ref. 4)] to produce the hydrated electron in bulk water, e^-(aq), versus the photon energy required [12.6 eV (Ref. 5)] to produce $e^-(g)$ from an isolated water molecule, i.e., to ionize it. Collective interactions enable the electron to exist in states that are less localized than, for instance, the valence orbitals of water molecules. These less localized states range from the ground state, bulk hydrated electron, which is thought to have a radius of gyration[6] of 2.4 Å at room temperature, to less localized *p*-like excited states, to delocalized conduction band electrons. Hydrated electron clusters are valuable probes for following the development of the collective interactions of solvation, since $(H_2O)^-_n$ cluster species must grow into e^-(aq) as $n \to \infty$.

Photoelectron spectra are recorded by crossing a fixed frequency laser beam (488.0 nm or 2.541 eV in this work) and a mass selected beam of anions. Photodetached electrons are counted as a function of electron kinetic energy which is recast as electron binding energy by the difference between the photon energy and the measured electron kinetic energy. Experimental conditions have been given previously.[7–10] The full line shapes of various species in the photoelectron spectra of hydrated electron clusters have been characterized in this work, as compared with our original presentations of the same data[7–10] which focused only on peak centers of the dominant spectral features. This approach allows the spectra of different isomeric species to be untangled and their relative intensities to be quantified. The electron binding energies of the isomeric species that we observed fall into three groups which we denote as dipole boundlike, intermediate, and bulk embryonts (species which grow smoothly with size into the bulk hydrated electron). This evolution reveals a general role for dipole binding and diffuse electron states in the formation of hydrated electrons. In the course of this work, we have also identified vibrational peaks in the blue asymmetric tails of these spectra. The behavior of these peaks with cluster size and upon deuteration, as well as the similarity of the photoelectron line shapes to absorption line shapes, provide new experimental clues to the molecular nature of the blue asymmetric tail of bulk hydrated electron absorption spectra. Most importantly, the results presented here have important consequences for our understanding of the energetics of bulk water in the region of the conduction band and enable the extrapolation of the entire photoelectron line shape to bulk. These latter two topics will be subjects of a subsequent paper.

This paper is organized as follows. It begins with a description of the line shape fitting functions utilized, followed by a presentation of the fitted spectra and a tabulation of the line shape parameters. Next, the electron binding energies of all peak centers are plotted against $n^{-1/3}$ (where n is the number of water molecules in the cluster) in order to see the grouping of various species and to identify the nature of each group. Then, we discuss several issues associated with line

a)Author to whom correspondence should be addressed. Electronic mail: coe.1@osu.edu
b)Author to whom correspondence should be addressed. Electronic mail: kbowen@jhu.edu

shapes including the engulfing of vibrational peaks and the possible meaning of the similarity between photoelectron and absorption line shapes. Finally, we discuss surface versus internal excess electron state issues which bear directly on the applicability of extrapolating these results to bulk. In effect, the present paper is a full paper, work up of data which we had previously published only in brief communicationlike venues.

FITTING CLUSTER ANION SPECTRA TO THE GAUSSIAN-LORENTZIAN EMPIRICAL FORM

The photoelectron spectra were fit with a simple Gaussian-Lorentzian, empirical fitting function[6] that is well known to give good fits to the bulk absorption spectrum of e^-(aq). Ultimately, the justification for this is that it works very well, i.e., there are almost no systematic deviations and the standard deviation of the fit is consistent with the noise in the data. It may seem surprising that the same empirical functional form[6] works for both the wavelength-fixed photoelectron spectra and the wavelength-scanned absorption spectra of hydrated electrons, but it is certainly not a coincidence as it works over the whole range of cluster sizes. We speculate that both the absorption and photoelectron spectra are dominated by the projection of the excess electron, ground state, solvent configurations onto the excited state curves in a solvation coordinate, i.e., by the Franck-Condon factors of solvent orientation. The photoelectron line shape parameters are determined in this work so they may be compared to absorption line shapes (regarding the nature of the excited states) in a subsequent paper.

Typically, the spectra of hydrated electron species are dominated by a single peak, i.e., the electronic origin, which is sometimes accompanied by smaller vibrational features of the neutral product. The fitting function, $I(E)$, for the electronic origins has a Gaussian form to the low electron binding energy side of the origin peak and a Lorentzian form to the high electron binding energy side. All origins were fit using the first term on the right hand side of Eq. (1), and any vibrational features were fit by adding one or more Gaussians (indexed by i) to the origin as follows:

$$I(E) = Ae^{-(1/2)(E - E_{\max}/\sigma_G)^2} + \sum_i A_i e^{-(1/2)(E - E_{\max,i}/\sigma_{G,i})^2}, \quad \text{if } E \leqslant E_{\max}$$

$$I(E) = \frac{A}{1 + \left[\frac{(E - E_{\max})}{\sigma_L}\right]^2} + \sum_i A_i e^{-(1/2)(E - E_{\max,i}/\sigma_{G,i})^2}, \quad \text{if } E \geqslant E_{\max}, \tag{1}$$

where $E_{\max}$ is the energy position of the origin's intensity maximum (vertical detachment energy), σ_G is the Gaussian standard deviation characterizing the origin's width on the low energy side of the peak (full width at half maximum divided by 2.354 for a full Gaussian line shape), σ_L is the origin's Lorentzian width parameter characterizing the high energy side (half width at half maximum for a full Lorentzian line shape), and A is the intensity maximum. The subscripted index (i) distinguishes the Gaussian parameters of the vibrational peaks ($E_{\max,i}$, $\sigma_{G,i}$, and A_i) from those of origins. Since bulk hydrated electron absorption spectra are known to have been fit with multiple combinations[11] of Gaussians and Gaussian-Lorentzian line shapes, it is important to point out that the photoelectron line shapes of these species have not been observed to change with any variations of ion source conditions (no resolved negative ion vibrations) and corresponding isomer populations, i.e., there is no evidence for other isomers in the smooth tails of these line shapes. Deuteration was key in distinguishing the peaks that were observed in the tails as vibrational. To illustrate the importance of deuteration, note the two higher electron binding energy peaks in the dimer anion spectra (top of Fig. 1). They shift dramatically with deuteration showing that they are vibrational in nature (a H–O–H bend and an O–H stretch), while the lowest electron binding energy peak barely shifts indicating that it is an electronic origin. The

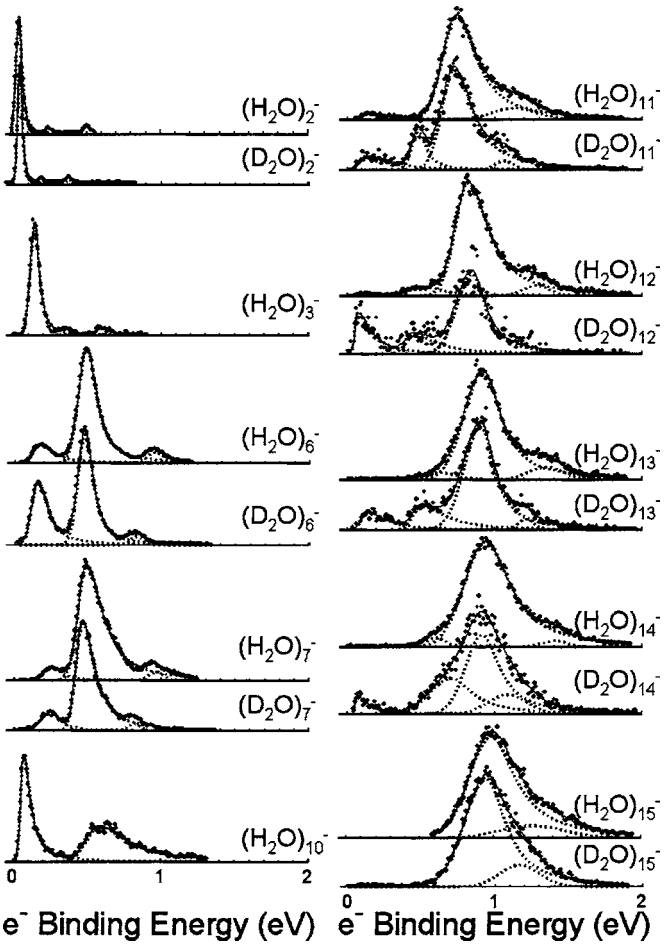

FIG. 1. Full range, simultaneous fits of all species in $(H_2O)_n^-$ (n=2, 3, 6, 7, 10–15) photoelectron spectra (solid line). The data were recorded with 2.540 eV laser photons, 8.5 meV bins in electron binding energy, and a resolution of 0.020 eV in electron binding energy. Fully deuterated spectra are overlapped with their corresponding nondeuterated spectra in order to identify origins and vibrational features and to show the increase in intensity of the lower electron binding energy species upon deuteration. Decomposed peak shapes are shown with dotted lines. Origins were fit to the same empirical form used to fit the hydrated electron's bulk absorption spectrum, namely, a Gaussian to the low binding energy side of the maximum and a Lorentzian to the high binding energy side as given by Eq. (1).

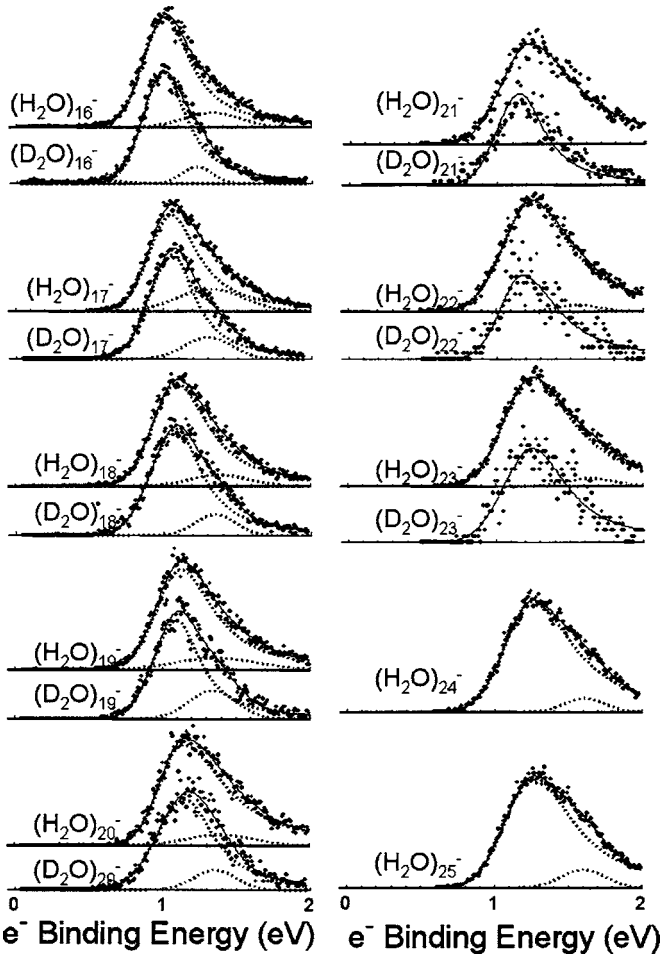

FIG. 2. Full range, simultaneous fits of all species in $(H_2O)_n^-$ (n=16–25) photoelectron spectra (solid line).

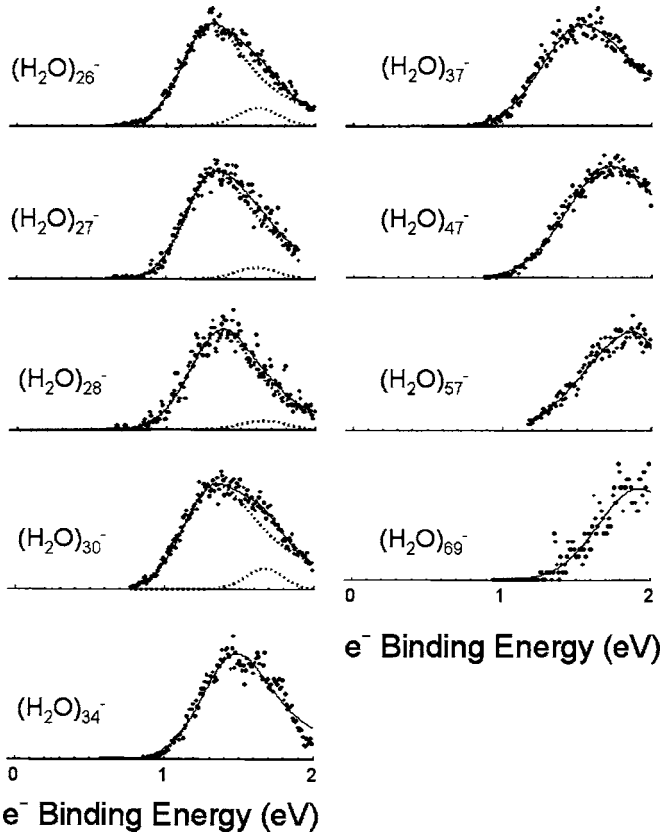

FIG. 3. Full range, simultaneous fits of all species in $(H_2O)_n^-$ (n=26–28, 30, 34, 37, 47, 57, 69) photoelectron spectra (solid line).

vibrational peaks identified in the spectra at larger cluster size are all O–H stretches that shift relative to the origins by a factor of $\sqrt{2}$ on average. The deuterated spectra have been placed directly underneath the nondeuterated spectra in Figs. 1–3 so that readers can independently inspect the isotopic shifts. Since many spectra displayed multiple types of species, i.e., multiple electronic origins were evident upon deuteration, they were simultaneously fit with each species represented by its own set of Eq. (1) parameters. The photoelectron fit parameters are given in Tables I–III (a different table for each identified group), while the fitted spectra are given in Figs. 1–3. If no σ_L parameter is given in the table, then that peak is vibrational and was fit to a Gaussian, rather than the Gaussian/Lorentzian form of the first term in Eq. (1). The fitted line shape of each peak was numerically integrated and the fractional contribution of each peak's area to the total is tabulated in the final column of Tables I–III.

IDENTIFYING AND GROUPING SPECTRA

All photoelectron peak centers (E_{max}) in the cluster data set have been plotted against $n^{-1/3}$ in Fig. 4. The parameter $n^{-1/3}$ is proportional to the inverse of cluster radius. It has the value of one when there is a single water molecule in the cluster and the value of zero when an infinite number of water molecules are present, as at bulk. The peaks fall into groups (circled and labeled in Fig. 4) by virtue of their energetics and trends with cluster size. Note that we see as many as three different types of species in a single photoelectron spectrum in the size range of $n \leqslant 16$.

The first group is identified as dipole boundlike states by virtue of their very small electron binding energies, and the fact that their smallest members (n=2,3) are well characterized as ground state, dipole bound anions with diffuse electron clouds.[7–10,12–14] Species in the dipole boundlike group exhibit a relatively flat trend in electron binding energy with increasing cluster size and are observed in the range of n =2–16. Their integrated spectral areas go from 100% at n =2 to 0% for $n>16$, as these species give way to more stable species with increasing cluster size. The hydrated electron clusters at n=2, 3, 6, 7, and 10 have more mass-spectral abundance than their adjacent size cluster anions, and similar results to this work have been observed by Kim *et al.*[15] In addition, however, they[15,16] have also contributed photoelectron spectra of the less abundant sizes at n=3, 4, 5, 8, and 9 including multiple isomers where the species they labeled[15] as isomer I correspond to this group. They observed three weakly bound species, described as diffuse-electron states, at n=4 (Ref. 16) suggesting the possibility of more discriminating classifications of these species. This grouping has also been recently studied by Verlet *et al.*[17] with still colder expansion conditions (due to higher expansion pressures than we had used), where they observed low electron binding energy species in $(D_2O)_n^-$ from n=11–35 (called isomer III by them). Thus, members of this grouping are now available

TABLE I. Line shape fit parameters of the dipole boundlike group for $(H_2O)_n^-$ and $(D_2O)_n^-$ photoelectron spectra as defined in Eq. (1). Spectra were fit from 0–2.2 eV in electron binding energy above which one can see evidence of reduced electron transmission. The peaks are identified as "origin" for the transition from the anion's ground vibrational state to the neutral's ground vibrational state, and "bend" or "stretch" for transition from the anion's ground state to the neutral's vibrational excited state. Estimated standard deviations from the fitting procedure alone are given in parenthesis as the least significant figures. These errors underestimate the actual errors as judged by global fits of the parameters. If no value for σ_L is given, then the peak was fit to a Gaussian rather than a Gaussian/Lorentzian form.

Species	Peak type	σ_G Gaussian peak width (eV)	σ_L Lorentzian peak width (eV)	E_{max} peak center (eV)	A peak intensity (e^- counts)	Integrated relative peak area
$(H_2O)_2^-$	Origin	0.02147(28)	0.0223(4)	0.04272(25)	4839(40)	0.890
	Bend	0.023(5)		0.249(6)	214(38)	0.037
	Stretch	0.030(4)		0.504(4)	327(33)	0.073
$(D_2O)_2^-$	Origin	0.0175(16)	0.01529(20)	0.04521(14)	6946(43)	0.930
	Bend	0.0132(33)		0.1940(4)	213(46)	0.021
	Stretch	0.0223(30)		0.375(4)	303(35)	0.049
	Offset				113(7)	
$(H_2O)_3^-$	Origin	0.0302(5)	0.0363(7)	0.1440(4)	147.9(14)	0.904
	Bend	0.030(10)		0.374(12)	5.0(14)	0.024
	Stretch	0.053(8)		0.611(9)	8.4(11)	0.072
$(H_2O)_6^-$	Origin	0.0461(14)	0.0987(27)	0.1728(15)	300(5)	0.143
$(D_2O)_6^-$	Origin	0.0448(6)	0.0811(11)	0.1614(6)	566(4)	0.379
$(H_2O)_7^-$	Origin	0.055(5)	0.072(8)	0.262(5)	146(8)	0.066
$(D_2O)_7^-$	Origin	0.0698(27)	0.0647(34)	0.2565(25)	89.0(22)	0.130
$(H_2O)_{10}^-$	Origin	0.0185(4)	0.0569(9)	0.0694(4)	192.9(18)	0.428
$(H_2O)_{11}^-$	Origin	0.045(10)	0.185(26)	0.137(11)	23.8(21)	0.044
$(D_2O)_{11}^-$	Origin	0.040(7)	0.186(20)	0.124(8)	15.7(11)	0.101
$(H_2O)_{12}^-$	Origin	0.022(17)	0.099(5)	0.095(19)	6.0(18)	0.009
$(D_2O)_{12}^-$	Origin	0.0165(25)	0.107(8)	0.0685(28)	13.8(7)	0.205
$(D_2O)_{13}^-$	Origin	0.042(5)	0.152(13)	0.139(6)	14.2(8)	0.105
$(D_2O)_{14}^-$	Origin	0.016(4)	0.087(12)	0.070(4)	14.8(12)	0.053
$(D_2O)_{16}^-$	Origin	0.063(31)		0.129(36)	3.8(15)	0.007

from $n=2-35$. Notably, Johnson and co-workers have measured infrared spectra for numerous small-sized clusters[18,19] (particularly with argons attached for cooling) yielding detailed structural information and the opportunity for comparison with theoretical calculations of diffuse-electron, hydrogen-bonding networks, such as those of K. S. Kim and co-workers[15,20–24] and Jordan and co-workers.[25,26]

The second group, the intermediate states, has electron binding energies that are intermediate between the dipole boundlike states and those of the most stable group. Candidates for these species have been considered theoretically[21,26,27] and experimentally.[26] They appear in the present work in the range of $n=6-16$, they dominate at $n=6$ and 7, and they give way to a more stable group in the range of $n=11-16$. Kim *et al.*[15] obtained similar results to this work at $n=6$, 7, and 10 (they called these isomer II) and have also found intermediate species at $n=3$, 5, 8, and 9. The work of Verlet *et al.* with cold expansions[17] found intermediate species from $n=11-200$ (called isomer II). They observed a transition over the range of $n=20-50$ suggesting the need for yet more discriminating classifications of these species. Their work overlapped with the present studies in the range of $(D_2O)_n^-$ with $n=11-23$. Notably, both studies find the same three isomers at $n=11$ and 13, providing further justification for the general classification into three groups. At the smaller intermediate isomer sizes, infrared spectra have also been recorded,[18,26,28] and there is the prospect of detailed structural information by comparison to theoretical calculations.[18,20,22,25,26,29] More "strongly bound surface states" have been observed in simulations where "surface states are localized within what might be called surface cavities"[30] Such structures may correspond to the larger clusters in this grouping. The larger intermediate cluster anions have been suggested[17] to arise from "electron attachment to ice nanocrystals," where solvent rearrangements to more-internalized forms have been inhibited by low temperatures. In general, the intermediate species are favored by deuteration and lower temperatures which suggest a kinetic role in their observation over more internalized structures.

We designate the third group as bulk embryonts because their properties grow smoothly with increasing cluster size into those of the bulk hydrated electron. They start at $n=11$ (or possibly at 10) and dominate at all larger sizes under the conditions of our ion source (as examined up to $n=69$). This group has an electron binding energy versus cluster size trend that is very close to that expected of bulk-correlated hydrated electron cluster species (based on the dielectric properties of ice or water).[8,31] Verlet *et al.*[17] have extended the range of this group with $(D_2O)_n^-$ from $n=11$ to 125. Warmer source conditions favor this group and the larger

TABLE II. Line shape fit parameters of the intermediate group for $(H_2O)_n^-$ and $(D_2O)_n^-$ photoelectron spectra as defined in Eq. (1). The peaks are identified as "origin" for the electronic origin or as "bend" or "stretch" if they are vibrations. Estimated standard deviations from the fitting procedure alone are given in parenthesis as the least significant figures. If no value for σ_L is given, then the peak was fit to a Gaussian rather than a Gaussian/Lorentzian form.

Species	Peak type	σ_G Gaussian peak width (eV)	σ_L Lorentzian peak width (eV)	E_{max} Peak center (eV)	A peak intensity (e^- counts)	Integrated relative peak area
$(H_2O)_6^-$	Origin	0.05683(25)	0.0778(4)	0.48972(24)	1861(5)	0.804
	Stretch	0.05457(24)		0.9561(23)	173(5)	0.053
$(D_2O)_6^-$	Origin	0.0491(4)	0.0628(5)	0.4813(3)	1010(4)	0.591
	Stretch	0.0425(32)		0.830(4)	76(4)	0.030
$(H_2O)_7^-$	Origin	0.0548(6)	0.1320(12)	0.4889(6)	1320(7)	0.904
	Stretch	0.050(5)		0.966(7)	95(9)	0.030
$(D_2O)_7^-$	Origin	0.0427(4)	0.0986(7)	0.4633(4)	526.6(22)	0.845
	Stretch	0.037(4)		0.815(5)	33.9(29)	0.025
$(H_2O)_{10}^-$	Origin	0.0824(25)	0.239(6)	0.5812(27)	61.7(9)	0.572
$(D_2O)_{11}^-$	Origin	0.046(3)	0.065(4)	0.4824(27)	43.4(15)	0.132
$(H_2O)_{12}^-$	Origin	0.117(11)	0.145(16)	0.535(10)	21.0(12)	0.068
$(D_2O)_{12}^-$	Origin	0.057(10)	0.182(24)	0.457(11)	6.1(5)	0.171
$(H_2O)_{13}^-$	Origin	0.115(10)		0.635(13)	19.8(15)	0.043
$(D_2O)_{13}^-$	Origin	0.061(5)	0.208(12)	0.506(5)	18.7(7)	0.189
$(H_2O)_{14}^-$	Origin	0.095(8)	0.064(9)	0.615(7)	25.1(15)	0.036
$(D_2O)_{14}^-$	Origin	0.144(6)	0.177(8)	0.706(5)	29.1(7)	0.300
$(H_2O)_{16}^-$	Origin	0.06(4)		0.54(5)	2.8(17)	0.004
$(D_2O)_{16}^-$	Origin	0.14(4)		0.60(5)	4.1(10)	0.018

cluster sizes in their work follow the same bulklike trend that was observed in the original photoelectron experiments of Coe *et al.*[8] Clearly, excess electrons in water clusters sense multiple minima on their potential energy landscapes. The recent high stagnation pressure studies of Verlet *et al.* confirmed the photoelectron features that we had observed and contributed many more, most notably the surface states of the large water cluster anions.

LINE SHAPE ISSUES

The peaks (identified as dipole boundlike, intermediate, or bulk embryont) shift in energy very little upon deuteration as expected for electronic origins. However, an additional group of peaks has been identified in Fig. 4 as vibrational in character because they shift systematically upon deuteration. The energy difference between the vibrational peaks and their corresponding origins defines a vibrational frequency which is plotted (in units of cm^{-1}) in Fig. 5 versus cluster size. At small cluster sizes, $n=2$, 3, 6, 7, and 11, the vibrational spacing corresponds to an O–H stretch and the trend with cluster size is flat. By $n=11$, however, the vibrational spacing in the bulk embryont group begins to smoothly diminish with increasing cluster size until it is eventually engulfed by the Lorentzian broadening of the electronic origin. There is a significant $\sqrt{2}$ isotope effect at all sizes where a vibrational peak has been found. Since, it becomes statistically difficult to identify the vibrational peak as cluster size increases, clusters in the range of $n=20-30$ were fit both with and without a vibrational peak and both results are given in Table III (see "alt. fit"). Above $n=30$, the vibrational peak could not be discerned from the Lorentzian tail. Solvation of ions generally localizes charge and vibrational frequencies of the anionic chromophore will shift to their condensed phase values with increased clustering. The current observations, with an electron rather than molecular anion, constitute the reverse of such general expectations (not seen before in photoelectron studies) and may represent a signature of electronic-vibrational mixing. More evidence for electronic-vibrational mixing comes from the effect of deuteration on the line shape of the photoelectron spectra. Deuteration has no effect on the low energy, Gaussian side of the line shapes, but produces an average reduction in the width of the blue asymmetric tails (σ_L) of the cluster photoelectron spectra by $\sim$0.06 eV (even after vibrational peaks are no longer discernible), which is similar to that of the bulk hydrated electron's absorption spectrum. Additionally, the resonance Raman spectra of the bulk hydrated electron recorded by Tauber and Mathies,[32] as well as enhancements in IR spectral intensities seen in spectra of hydrated electron clusters by dissociation techniques,[18,33] provide further evidence of strong electronic-vibrational mixing.

The above observations are relevant to a molecular explanation of the much-debated, blue asymmetric tail in the bulk absorption spectra of the hydrated electron. We now suspect that the blue asymmetric tailing is not due to the embedding of excited p states in the continuum, but rather to a common, ultrafast solvent response upon photoexcitation to either a less-localized p state or the conduction band. The-

TABLE III. Line shape fit parameters of the bulk embryont group for $(H_2O)_n^-$ and $(D_2O)_n^-$ photoelectron spectra as defined in Eq. (1). The peaks are identified as "origin" for the electronic origin or as "bend" or "stretch" if they are vibrations. Estimated standard deviations from the fitting procedure alone are given in parenthesis as the least significant figures. These errors underestimate the actual errors as judged by global fits of the parameters, but they provide a good sense of relative variations through the data set. Globally, we find the estimated standard deviations of E_{max}, σ_G, and σ_L, and σ_L to be 0.035, 0.013, and 0.06 eV, respectively. If no value for σ_L is given, then the peak was fit to a Gaussian rather than a Gaussian/Lorentzian form. For $n>16$ there was only one species present in each photoelectron spectrum, but it was often fit with and without a vibrational feature as indicated with "alt. fit."

Species	Peak type	σ_G Gaussian peak width (eV)	σ_L Lorentzian peak width (eV)	E_{max} peak center (eV)	A peak intensity (e^- counts)	Integrated relative peak area
$(H_2O)_{11}^-$	Origin	0.0962(8)	0.1626(14)	0.7437(8)	426.8(19)	0.860
	Stretch	0.149(6)		1.131(8)	47.1(17)	0.096
$(D_2O)_{11}^-$	Origin	0.0830(14)	0.1507(25)	0.7244(14)	114.4(10)	0.737
	Stretch	0.063(10)		1.062(12)	10.1(14)	0.030
$(H_2O)_{12}^-$	Origin	0.0874(7)	0.1667(13)	0.8200(8)	275.2(12)	0.875
	Stretch	0.085(5)		1.283(7)	26.0(15)	0.048
$(D_2O)_{12}^-$	Origin	0.102(3)	0.110(4)	0.8465(29)	26.2(5)	0.624
$(H_2O)_{13}^-$	Origin	0.1267(10)	0.1459(14)	0.9210(9)	308.5(15)	0.880
	Stretch	0.117(6)		1.347(7)	35.9(15)	0.077
$(D_2O)_{13}^-$	Origin	0.1126(15)	0.1124(20)	0.9053(13)	83.8(7)	0.677
	Stretch	0.053(7)		1.214(9)	8.6(10)	0.029
$(H_2O)_{14}^-$	Origin	0.1436(9)	0.1974(13)	0.9400(8)	300.1(11)	0.940
	Stretch	0.090(9)		1.407(11)	16.9(14)	0.025
$(D_2O)_{14}^-$	Origin	0.1114(23)	0.144(3)	0.9156(22)	64.2(8)	0.528
	Stretch	0.133(7)		1.088(9)	15.7(8)	0.119
$(H_2O)_{15}^-$	Origin	0.1455(13)	0.1999(20)	0.9827(12)	373.2(19)	0.886
	Stretch	0.212(9)		1.261(12)	44.2(17)	0.114
$(D_2O)_{15}^-$	Origin	0.1452(11)	0.1572(15)	0.9343(10)	192.1(9)	0.834
	Stretch	0.145(3)		1.152(4)	44.5(9)	0.166
$(H_2O)_{16}^-$	Origin	0.1466(14)	0.2119(23)	1.0072(14)	179.1(10)	0.888
	Stretch	0.189(9)		1.329(11)	23.3(9)	0.108
$(D_2O)_{16}^-$	Origin	0.1396(14)	0.1863(21)	0.9939(13)	162.7(9)	0.900
	Stretch	0.102(5)		1.221(7)	24.5(12)	0.075
$(H_2O)_{17}^-$	Origin	0.1473(14)	0.2226(23)	1.0509(14)	275.0(15)	0.804
	Stretch	0.222(5)		1.319(6)	63.4(13)	0.196
$(D_2O)_{17}^-$	Origin	0.1559(16)	0.1851(23)	1.0565(15)	114.3(7)	0.850
	Stretch	0.162(5)		1.301(7)	23.7(7)	0.150
$(H_2O)_{18}^-$	Origin	0.1612(17)	0.2606(29)	1.0908(17)	118.6(7)	0.911
	Stretch	0.201(12)		1.381(14)	13.8(7)	0.089
$(D_2O)_{18}^-$	Origin	0.1631(22)	0.211(3)	1.0717(21)	121.9(10)	0.849
	Stretch	0.155(6)		1.320(8)	29.4(10)	0.151
$(H_2O)_{19}^-$	Origin	0.1626(17)	0.2768(30)	1.1224(17)	138.8(8)	0.880
	Stretch	0.285(13)		1.367(16)	16.5(7)	0.120
$(D_2O)_{19}^-$	Origin	0.1553(26)	0.191(4)	1.0979(24)	48.3(5)	0.808
	Stretch	0.161(7)		1.342(8)	13.9(5)	0.192
$(H_2O)_{20}^-$	Origin	0.1554(21)	0.351(4)	1.1390(22)	90.2(6)	0.920
	Stretch	0.232(17)		1.392(20)	9.7(6)	0.080
Alt. fit	Origin	0.1635(20)	0.364(4)	1.1545(21)	97.0(6)	1.000
$(D_2O)_{20}^-$	Origin	0.191(4)	0.234(5)	1.160(3)	40.5(5)	0.881
	Stretch	0.144(10)		1.362(12)	9.0(5)	0.119
$(H_2O)_{21}^-$	Origin	0.1868(27)	0.378(6)	1.2141(28)	106.1(8)	1.000
$(D_2O)_{21}^-$	Origin	0.152(4)	0.202(6)	1.152(4)	25.9(4)	1.000
$(H_2O)_{22}^-$	Origin	0.1902(21)	0.319(4)	1.2409(21)	153.5(10)	0.975
	Stretch	0.131(22)		1.562(27)	8.8(13)	0.025
Alt. fit	Origin	0.1937(22)	0.335(4)	1.2469(22)	154.6(10)	1.000
$(D_2O)_{22}^-$	Origin	0.149(6)	0.290(11)	1.175(6)	14.3(3)	1.000
$(H_2O)_{23}^-$	Origin	0.1866(18)	0.347(4)	1.2422(18)	179.0(9)	0.963
	Stretch	0.163(17)		1.646(20)	12.8(11)	0.037
Alt. fit	Origin	0.1871(18)	0.386(4)	1.2431(19)	179.3(9)	1.000
$(D_2O)_{23}^-$	Origin	0.183(6)	0.305(11)	1.234(6)	15.4(3)	1.000

TABLE III. (*Continued.*)

Species	Peak type	σ_G Gaussian peak width (eV)	σ_L Lorentzian peak width (eV)	E_{max} peak center (eV)	A peak intensity (e^- counts)	Integrated relative peak area
$(H_2O)_{24}^-$	Origin	0.1859(19)	0.338(3)	1.2548(18)	254.6(13)	0.945
	Stretch	0.137(8)		1.608(10)	32.0(17)	0.055
Alt. fit	Origin	0.1929(21)	0.382(4)	1.2662(21)	257.7(15)	1.000
$(H_2O)_{25}^-$	Origin	0.1860(15)	0.3367(29)	1.2582(15)	270.1(12)	0.922
	Stretch	0.149(6)		1.602(7)	45.2(15)	0.078
Alt. fit	Origin	0.2005(20)	0.386(4)	1.2816(20)	277.6(15)	1.000
$(H_2O)_{26}^-$	Origin	0.1888(24)	0.325(5)	1.2946(24)	122.3(9)	0.921
	Stretch	0.140(8)		1.616(10)	21.6(11)	0.079
Alt. fit	Origin	0.2029(28)	0.371(6)	1.3190(28)	126.3(9)	1.000
$(H_2O)_{27}^-$	Origin	0.190(3)	0.340(7)	1.326(3)	77.0(7)	0.953
	Stretch	0.138(19)		1.610(23)	8.2(9)	0.047
Alt. fit	Origin	0.201(5)	0.358(7)	1.345(3)	79.3(7)	1.000
$(H_2O)_{28}^-$	Origin	0.216(5)	0.287(8)	1.373(5)	28.2(4)	0.955
	Stretch	0.15(3)		1.65(4)	2.5(5)	0.045
Alt. fit	Origin	0.223(5)	0.306(8)	1.387(5)	28.8(4)	1.000
$(H_2O)_{30}^-$	Origin	0.2095(29)	0.379(6)	1.3402(29)	119.0(9)	0.931
	Stretch	0.124(8)		1.669(10)	23.2(13)	0.069
Alt. fit	Origin	0.231(4)	0.422(8)	1.375(4)	123.1(10)	1.000
$(H_2O)_{34}$	Origin	0.224(4)	0.336(9)	1.484(4)	76.6(8)	1.000
$(H_2O)_{37}$	Origin	0.260(4)	0.460(12)	1.526(4)	89.2(8)	1.000
$(H_2O)_{47}$	Origin	0.287(3)	0.478(18)	1.718(3)	187.4(12)	1.000
$(H_2O)_{57}$	Origin	0.330(5)	NA[a]	1.884(4)	88.3(8)	1.000
$(H_2O)_{69}$	Origin	0.271(8)	NA[a]	1.924(9)	11.94(22)	1.000

[a]These spectra extended out of the photon range leaving little Lorentzian part to fit.

oretical treatments face the challenge of a non-Born-Oppenheimer linking of electronic and vibrational degrees of freedom in this problem.

To further explore this point, consider the unexpected similarity of the photoelectron spectral line shapes to bulk hydrated electron absorption line shapes. A frequency-scanned absorption (or photoemission) spectrum might be expected to have an integrated appearance compared to a fixed-frequency photoelectron spectrum which is further mediated by the gradual energy dependence of the transition moment integral. The similarity indicates that certain phenomena are commonly at work in defining the shape of both

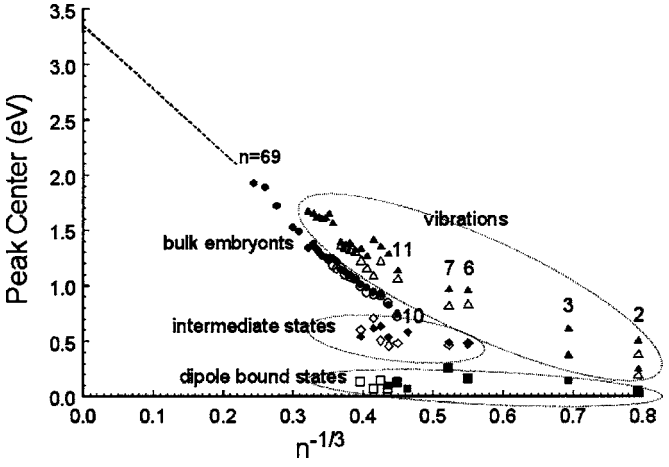

FIG. 4. Plot of all photoelectron peak centers vs $n^{-1/3}$ where n is the number of waters. Peaks discussed as groups in the text have been circled and labeled including dipole boundlike states (square symbols, lowest binding energies, surface states), intermediate states (diamond symbols) which step toward internalization, and bulk embryonts (circle symbols) which progress smoothly to bulk. The fully deuterated results are given with open symbols while the nondeuterated results are indicated with filled symbols. A set of vibrational peaks (triangle symbols) has also been identified by virtue of deuteration.

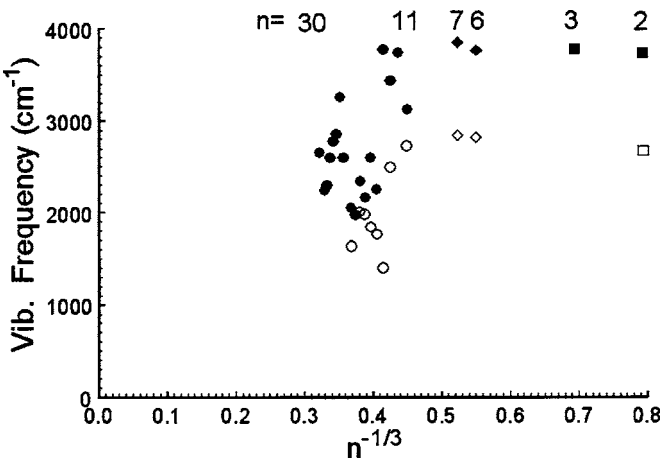

FIG. 5. Plot of the vibrational spacing in photoelectron spectra vs $n^{-1/3}$ where n is the number of waters. Dipole boundlike species are plotted with squares, intermediate species with diamonds, and bulk embryonts with circles. All $(H_2O)_n^-$ species are plotted with filled symbols, while $(D_2O)_n^-$ species are plotted with open symbols. From $n=2$ to 11, the vibration appears to be that of an asymmetric O–H stretch(s). From $n=11$, the vibrational interval reduces until the vibrational peak cannot be extracted from the origin at $n=\sim 30$. The spacing always reduces upon deuteration by $\sim\sqrt{2}$.

the absorption and photoelectron spectra. We propose that both the absorption and photoelectron spectra are dominated by the projection of the excess electron ground state solvent configurations onto the excited state potential curves in a solvation coordinate, i.e., by the Franck-Condon factors of solvent orientation. There is more to this similarity than just the general line shape. Solvent reorganization energies for removing an electron from water clusters are substantial in this system (estimated as ~0.7 eV at $n=11$ to ~1.7 eV at $n=\infty$) suggesting a possible role for relaxation of solvent configuration about charge upon excitation of the excess electron in the Lorentzian tails. At any given cluster size, the Lorentzian tails of the photoelectron spectra have the same value as the action/absorption spectra of Ayotte and Johnson.[33] The photoelectron line shape is the same as the absorption line shape at $n=11$, and then gradually separates as a p state gradually stabilizes[34–37] relative to the conduction band with increased cluster size. The blue asymmetric tails persist whether p states or the conduction band are accessed suggesting a nuclear motion component to the spectral tailing. These issues will be examined in more depth in a subsequent paper.

SURFACE VERSUS INTERNAL STATES IN HYDRATED ELECTRON CLUSTERS

Almost two decades ago, we recorded the first photoelectron spectra of water cluster anions, $(H_2O)_n^-$, for $n=2-69$. For $n\geqslant 11$, we found that a plot of our measured vertical detachment energies versus $n^{-1/3}$ extrapolated to reasonable bulk hydrated electron values with a predictable slope (based on the dielectric continuum equation presented by Landman and co-workers[38,39]). We interpreted this behavior[8,9] as suggesting that by $n=11$, these species had become embryonic hydrated electrons and that their excess electrons were either already internalized or beginning the process of internalizing. Certainly, for $n\geqslant 11$, the data implied some sort of significant kinship between water cluster anions and the bulk hydrated electron, realizing of course, that size effects would remain prevalent until very much larger sizes were reached.

This interpretation, however, disagreed with the pioneering quantum path integral, molecular dynamics simulations[30,39] of Landman and co-workers, as well as recent work by Turi *et al.*[40] Admirably, these investigators have taken on one of the most challenging theoretical problems in chemical physics, simultaneously tackling both diffuse electron states and many-body interactions in water. The calculated surface state vertical detachment energies (VDEs) of Landman and co-workers agreed with our measured bulk embryont VDEs over the $n=11-20$ size regime. Thus, based solely on a quantitative match between our measured VDEs and their calculated values, they proposed that we had observed surface and not internal states. This interpretation, based on a quantitative correspondence, was made despite the fact that calculated internal state VDEs extrapolated to a highly unrealistic bulk value with an equally unrealistic $n^{-1/3}$ slope.[41] Verlet *et al.* have shown[17] (see Fig. 3 in reference) that scaling by 60% gives a good correspondence with the experimental data. Similarly, the interior states of Turi *et al.* have an $n^{-1/3}$ slope of ~12 eV (about twice the 5.6 eV dielectric limit in water[31]). The simulations of Turi *et al.* find surface states falling below the experimental bulk embryont VDEs and lying close to the intermediate experimental group. One could have interpreted these results as being in reasonable accord with experiment given the uncalibrated model energetics. The authors, however, drew the opposite conclusion.

The calculations of Landman and co-workers predicted the size range over which the transition from surface to internal excess electron states should occur. Initially it was found to occur between $n=32-64$,[39] but subsequent work[30] suggested that the transition was occurring at $n>60$.[30] Since the predicted energy differences between the vertical detachment energies of internal versus surface states at a given size would be easily discernible experimentally, such a transition should have been evident as a discontinuity in plots of measured vertical detachment energy versus cluster size, n. However, neither our vertical detachment energy measurements[8] of the predominant species (bulk embryonts) from $n=11-69$, nor the action/absorption spectral maxima of Johnson and co-workers[33,42] from $n=11-50$ showed such a transition. Colder source conditions due to higher nozzle expansion pressures favor surface states[17] suggesting a kinetic barrier at low temperatures to the solvent reorientation associated with electron internalization, i.e., the warmer conditions of our experiment allow the solvent reorganization associated with internalization. In our warmer experiments, all three groups of species are in evidence in the size range of $n=11-16$. Thus, this is a critical region where such species are likely to have comparable free energy. Examining the full range/full line shape fits of Table I, one can identify 15 species (counting both light hydrogen- and deuterium-containing species) that qualify as part of the dipole boundlike group. Dipole bound species are now well known and have been explored in a number of experimental[43,44] and theoretical studies.[13,45] This group of species is represented at sizes, $n=2$, 3, 6, 7, 10–14, and 16 (and at $n=2-11$ in work by Kim *et al.*[15] and at $n=11-35$ in studies by Verlet *et al.*[17]). As in the light hydrogen-based spectra, the integrated relative peak areas in the deuterated spectra exhibit a trend that starts at 100% for $n=2$ and falls to 0.7% in the spectrum of $n=16$. The dipole boundlike group gives way to more stable species as cluster size increases, and disappears, under our source conditions, for $n>16$. In addition, 12 other species are observed that are grouped as intermediate states at $n=6$, 7, 10–14, and 16 (and at $n=3-11$ by Kim *et al.*[15] and up to $n=150$ by Verlet *et al.*[17]) However, under our warmer source conditions, both the dipole boundlike and the intermediate states become less prominent than the bulk embryonts by $n=11$. While more complicated than originally predicted by virtue of the intermediate states, the theoretically predicted surface to internal state transition is indeed observed. It just occurs around $n=11$ at our source conditions, rather than at some larger size.

In the course of sorting through these issues, it is notable that Barnett *et al.* proposed, after their initial predictions, the existence of a second class of surface states.[30] They referred

to these as "strongly bound surface states," saying surface states are localized within what might be called surface cavities. They then proposed that these could give rise to internal-like $n^{-1/3}$ trends and suggested that these were the species of our original photoelectron report[8] for $n \geqslant 11$. It seems likely[17] that these species are good candidates for the intermediates states, particularly the ones observed at larger cluster sizes.

At the cluster sizes of $n=6$ and 7, two types of states are observed which deserve additional comment in order to place them in perspective. Years ago, when we first discovered that $n=6$ and 7 have two distinct isomers each, we speculated that the lower electron binding energy states of each might be the more internalized ones, because they lay on the bulk $n^{-1/3}$ line.[7–9] This, however, did not properly account for the excess electron's contribution to cluster volume. In accordance with the arguments already presented on excess electron well depth and hydrogen bonding, the observed intensities upon deutration, the studies of Kim *et al.*,[15] and the calculations of K. S. Kim and co-workers,[22,24] it is now clear that the higher electron binding energy isomers are the more internalized ones, and hence should be considered to be members of the intermediate group. The less stable species should be placed in the dipole boundlike group, although the simple three group scheme may be insufficient for classifying these particular species.

We note in our data still another basis for arguing that a transition from surface to internal excess electron states occurs at moderate water cluster anion sizes. A redetermination of the excess electron's bulk hydration entropy by Han and Bartels[46] concluded that "hydrated electrons must be enormously effective 'structure-breaking' ions." When two or more groups of species are represented in a particular photoelectron spectrum, we observe that the lower electron binding energy species are always more abundant (their peaks are relatively more intense) in the deuterated version of the spectrum than in the light hydrogen version (see the last column of Tables I–III). That is, the effect of deuteration is to induce a greater relative stabilization (and thus abundance) of the lower electron binding energy species over the higher electron binding energy species in the same spectrum. Given that higher electron binding energies must be positively correlated with the depth of excess electron wells, this implies that the lower electron binding energy species must have larger zero point energies than the more stable species with higher electron binding energies in order to explain this effect. The relative stabilization upon lowering the zero point energy due to deuteration is greater in the species with both a higher zero point energy and shallower excess electron wells, i.e., the low electron binding energy species. Since all of the species in the same spectrum have the same number of water molecules, this can only come about due to stronger hydrogen bonding in the lower (as compared to the higher) electron binding energy species. As implied by Han and Bartels, the process of hydrating (internalizing) and electron in water is one of reducing the hydrogen bonding between nearby water molecules. Thus, the change in relative peak intensities upon deuteration is consistent with a transition from strongly hydrogen bonded species with weakly bound excess electrons to less strongly hydrogen bonded structures with more deeply bound excess electrons. Consequently, the transition from dipole boundlike, to intermediate, to embryonic species is associated with increasing excess electron internalization. The group of species herein identified as bulk embryonts are the most internalized states which evolve with size into bulk hydrated electrons. Our picture of the electron internalization process is one in which the excess electron density is gradually drawn into the interior of the $(H_2O)^-_{n\geqslant 11}$ embryonts as they grow in size.

There has been additional theoretical work that sheds light on internalization. Since the hydrated electron, e^-(aq), is inherently an internal state at bulk, one expects the excess electrons in water cluster anions to internalize with increased cluster size. This does not mean that the excess electrons in the smallest $(H_2O)^-_n$ clusters are necessarily internalized, nor does it mean that the smallest bulk embryonts, such as at $n=11$, are yet fully internalized. Kim *et al.* have performed[27] *ab initio* calculations (HF, MP2, and B3LYP with 6-311++G^{**} basis sets) on the $(H_2O)^-_{12}$ cluster and found a variety of structures with various degrees of excess electron internalization to have comparable stabilities. They found a "partially internal" structure to have good agreement with the bulk embryont vertical detachment energy. There are also some hybrid density functional calculations (B3LYP/6-311++G^{**}) by Khan[47] that bear on the internalization of an excess electron in distorted cages of 24 water molecules. Three $(H_2O)^-_{24}$ isomers were found, two of which were surfacelike, while the third one was an interior state. It was noted that the isomer with its vertical detachment energy closest to our bulk embryont experimental value was the interior state. Such studies face the daunting challenges of dealing with diffuse electrons and a vast number of possible hydrogen bonding structures for many possible frameworks.[48] As computer power increases, more *ab initio*-based pictures are emerging of the excess electron and the fluxional nature of its cavity.[49,50]

There has also been a great deal of pertinent work in the time domain. Simulations[50,51] and ultrafast experiments[37,52] at bulk have demonstrated p states lying below the conduction band, while two-photon, ultrafast photoelectron experiments[34–36] have accessed p states lying below the vacuum level in hydrated electron clusters. After years of debate, it is clear[53] that there are significant contributions to the absorption spectrum from p states lying below the conduction band. Upon considering their dynamic measurements, both Paik *et al.*[35] and Bragg *et al.*[36] concluded that internalized excess electron states were likely to exist in the water cluster anions they had studied.

CONCLUSION

Cluster anion sizes at $n=2$ and 3 have long been characterized as dipole bound states.[14,20,44] In light of the observation of surface states over a wide range of $n \geqslant 11$ cluster sizes,[17] our own observations of low electron binding energy states over a smaller range of cluster sizes ($n=2-16$), and other observations at $n \leqslant 11$,[15] we interpret both the dipole boundlike and intermediate states described in the present

paper as surface states at different stages along the road to internalization. The coincident observation[17] of several types of larger-size surface states along with a group similar to those herein called bulk embryonts enables a more definitive conclusion that our previously observed high VDE, water cluster anion spectra are indeed due to internally solvated electron states, i.e., bulk embryonts. Verlet *et al.* and ourselves have both seen and identified three types (groupings) of water cluster anion, excess electron states, i.e., an internal state and two kinds of surface states. Taken together, these studies resolve a long debate over the nature of the excess electron in water cluster anions. In the finite size regime, internalizing states of water cluster anions are embryos of bulk hydrated electrons.

ACKNOWLEDGMENTS

We thank Dan Neumark and Ahmed Zewail for discussions on this topic. K.B. thanks the National Science Foundaiton for support of this work under grant number CHE-0517337 and all previous NSF grants. J.V.C. and S.M.W. thank the ACS PRF (38502-AC5) and the NSF (CHE-0413077).

[1] H_2O^- has been observed, but it is most likely an ion-molecule complex.
[2] L. J. deKonig and N. M. M. Nibbering, J. Am. Chem. Soc. **106**, 7971 (1984).
[3] P. Han and D. M. Bartels, J. Phys. Chem. **94**, 5824 (1990).
[4] D. M. Bartels and R. A. Crowell, J. Phys. Chem. A **104**, 3349 (2000).
[5] *CRC Handbook of Chemistry and Physics*, 78th ed. (CRC, Boca Raton, 1997).
[6] F.-Y. Jou and G. R. Freeman, J. Phys. Chem. **83**, 2383 (1979); T. R. Tuttle and S. Golden, J. Chem. Soc., Faraday Trans. 2 **77**, 873 (1981).
[7] J. V. Coe, Ph.D. thesis, The Johns Hopkins University, 1986.
[8] J. V. Coe, G. H. Lee, J. G. Eaton, S. T. Arnold, H. W. Sarkas, K. H. Bowen, C. Ludewigt, H. Haberland, and D. R. Worsnop, J. Chem. Phys. **92**, 3980 (1990).
[9] S. T. Arnold, J. V. Coe, J. G. Eaton *et al.*, in *The Chemical Physics of Atomic and Molecular Clusters*, edited by G. Scoles (Elsevier, Amsterdam, 1990), p. 467; G. H. Lee, S. T. Arnold, J. G. Eaton, H. W. Sarkas, K. H. Bowen, C. Ludewigt, and H. Haberland, Z. Phys. D: At., Mol. Clusters **20**, 9 (1991); A. W. Castleman, Jr. and K. H. Bowen, Jr., J. Phys. Chem. **100**, 12911 (1996); J. V. Coe, A. D. Earhart, M. H. Cohen, G. J. Hoffman, H. W. Sarkas, and K. H. Bowen, J. Chem. Phys. **107**, 6023 (1997).
[10] S. T. Arnold, Ph.D. thesis, The Johns Hopkins University, 1994.
[11] F.-Y. Jou and G. R. Freeman, Can. J. Chem. **57**, 591 (1979).
[12] D. M. Chipman, J. Phys. Chem. **83**, 1657 (1979); R. N. Barnett, U. Landman, S. Dhar, N. R. Kestner, J. Jortner, and A. Nitzan, J. Chem. Phys. **91**, 7797 (1989).
[13] A. Wallqvist, D. Thirumalai, and B. J. Berne, J. Chem. Phys. **85**, 1583 (1986); M. Gutowski, P. Skurski, K. D. Jordan, and J. Simons, Int. J. Quantum Chem. **64**, 183 (1997).
[14] G. H. Lee, S. T. Arnold, J. G. Eaton, and K. H. Bowen, Chem. Phys. Lett. **321**, 333 (2000); D. M. A. Smith, J. Smets, Y. Elkadi, and L. Adamowicz, J. Chem. Phys. **107**, 5788 (1997).
[15] J. Kim, I. Becker, O. Cheshnovsky, and M. A. Johnson, Chem. Phys. Lett. **297**, 90 (1998).
[16] J.-W. Shin, N. I. Hammer, J. M. Headrick, and M. A. Johnson, Chem. Phys. Lett. **399**, 349 (2004).
[17] J. R. R. Verlet, A. E. Bragg, A. Kammrath, O. Cheshnovsky, and D. M. Neumark, Science **307**, 93 (2005).
[18] N. I. Hammer, J.-W. Shin, J. M. Headrick, E. G. Diken, J. R. Roscioli, G. H. Weddle, and M. A. Johnson, Science **306**, 675 (2004).
[19] C. G. Bailey, J. Kim, and M. A. Johnson, J. Phys. Chem. **100**, 16782 (1996).
[20] J. Kim, S. B. Suh, and K. S. Kim, J. Chem. Phys. **111**, 10077 (1999).
[21] S. Lee, J. Kim, S. J. Lee, and K. S. Kim, Phys. Rev. Lett. **79**, 2038 (1997).
[22] K. S. Kim, S. Lee, J. Kim, and J. Y. Lee, J. Am. Chem. Soc. **119**, 9329 (1997).
[23] S. Lee, S. J. Lee, J. Y. Lee, J. Kim, K. S. Kim, I. Park, K. Cho, and J. D. Joannopoulos, Chem. Phys. Lett. **254**, 128 (1996).
[24] K. S. Kim, I. Park, S. Lee, K. Cho, J. Lee, J. Kim, and J. D. Joannopoulos, Phys. Rev. Lett. **76**, 956 (1996).
[25] N. I. Hammer, J. R. Roscioli, M. A. Johnson, E. M. Myshakin, and K. D. Jordan, J. Phys. Chem. A **109**, 11526 (2005); E. M. Myshakin, K. Diri, and K. D. Jordan, *ibid.* **108**, 6758 (2004).
[26] P. Ayotte, G. H. Weddle, C. G. Bailey, M. A. Johnson, F. Vila, and K. D. Jordan, J. Chem. Phys. **110**, 6268 (1999).
[27] J. Kim, J. M. Park, K. S. Oh, J. Y. Lee, S. Lee, and K. S. Kim, J. Chem. Phys. **106**, 10207 (1997).
[28] C. G. Bailey, J. Kim, and M. A. Johnson, J. Phys. Chem. **100**, 16782 (1996).
[29] H. M. Lee, S. B. Suh, and K. S. Kim, J. Chem. Phys. **119**, 7685 (2003); H. M. Lee, S. B. Suh, and K. S. Kim, *ibid.* **118**, 9981 (2003).
[30] R. N. Barnett, U. Landman, G. Makov, and A. Nitzan, J. Chem. Phys. **93**, 6226 (1990).
[31] J. V. Coe, J. Phys. Chem. A **101**, 2055 (1997).
[32] M. J. Tauber and R. A. Mathies, J. Phys. Chem. A **105**, 10952 (2001).
[33] P. Ayotte and M. A. Johnson, J. Chem. Phys. **106**, 811 (1997).
[34] J. M. Weber, J. Kim, E. A. Woronowicz, G. H. Weddle, I. Becker, O. Cheshnovsky, and M. A. Johnson, Chem. Phys. Lett. **339**, 337 (2001).
[35] D. H. Paik, I. R. Lee, D.-S. Yang, J. S. Baskin, and A. H. Zewail, Science **306**, 672 (2004).
[36] A. E. Bragg, J. R. R. Verlet, A. Kammrath, O. Cheshnovsky, and D. M. Neumark, Science **306**, 669 (2004).
[37] P. Kambhampati, D. H. Son, T. W. Kee, and P. F. Barbara, J. Phys. Chem. A **106**, 2374 (2002).
[38] R. N. Barnett, U. Landman, C. L. Cleveland, and J. Jortner, Chem. Phys. Lett. **145**, 382 (1988); R. N. Barnett, U. Landman, C. L. Cleveland, and J. Jortner, J. Chem. Phys. **88**, 4421 (1988); R. N. Barnett, U. Landman, C. L. Cleveland, N. R. Kestner, and J. Jortner, *ibid.* **88**, 6670 (1988); R. N. Barnett, U. Landman, C. L. Cleveland, and J. Jortner, Phys. Rev. Lett. **59**, 811 (1987).
[39] R. N. Barnett, U. Landman, C. L. Cleveland, and J. Jortner, J. Chem. Phys. **88**, 4429 (1988).
[40] L. Turi, W. S. Sheu, and P. J. Rossky, Science **309**, 914 (2005).
[41] J. V. Coe, Int. Rev. Phys. Chem. **20**, 33 (2001).
[42] L. A. Posey, P. J. Campagnola, M. A. Johnson, G. H. Lee, J. G. Eaton, and K. H. Bowen, J. Chem. Phys. **91**, 6536 (1989).
[43] R. D. Mead, K. R. Lykke, W. C. Lineberger, J. Marks, and J. I. Brauman, J. Chem. Phys. **81**, 4883 (1984); K. R. Lykke, R. D. Mead, and W. C. Lineberger, Phys. Rev. Lett. **52**, 2221 (1984); J. H. Hendricks, S. A. Lyapustina, H. L. de Clercq, J. T. Snodgrass, and K. H. Bowen, J. Chem. Phys. **104**, 7788 (1996); J. H. Hendricks, H. L. de Clercq, S. A. Lyapustina, and K. H. Bowen, Jr., *ibid.* **107**, 2962 (1997).
[44] "Photoelectron Spectroscopy of Small Cluster Anions: Dipole Bound, Ground State Systems," J. H. Hendricks, H. L. de Clercq, S. A. Lyapustina, C. A. Fancher, T. P. Lippa, J. M. Collins, S. T. Arnold, G. H. Lee, and K. H. Bowen, in *Structures and Dynamics of Clusters, Proceedings of Yamada Conference XLIII*, edited by T. Kondow, K. Kaya, and A. Terasaki, Shimoda, Japan, 10–13 May 1995 (Universal Academy Press, Tokyo, 1996), Vol. 16, pp. 321–328.
[45] D. M. A. Smith, J. Smets, Y. Elkadi, and L. Adamowicz, Chem. Phys. Lett. **288**, 609 (1998); D. M. A. Smith, J. Smets, and L. Adamowicz, J. Chem. Phys. **110**, 3804 (1999); J. Smets, D. M. A. Smith, Y. Elkadi, and L. Adamowicz, Pol. J. Chem. **72**, 1615 (1998); D. M. A. Smith, J. Smets, Y. Elkadi, and L. Adamowicz, J. Chem. Phys. **109**, 1238 (1998); M. Gutowski, K. D. Jordan, and P. Skurski, J. Phys. Chem. A **102**, 2624 (1998); M. Gutowski and P. Skurski, J. Chem. Phys. **107**, 2968 (1997).
[46] P. Han and D. M. Bartels, J. Phys. Chem. **95**, 5367 (1991).
[47] A. Khan, J. Chem. Phys. **121**, 280 (2004).
[48] J.-L. Kuo, J. V. Coe, S. J. Singer, Y. B. Band, and L. Ojamae, J. Chem. Phys. **114**, 2527 (2001); M. D. Tissandier, S. J. Singer, and J. V. Coe, J. Phys. Chem. A **104**, 752 (2000).
[49] I. Park, K. Cho, S. Lee, K. S. Kim, and J. D. Joannopoulos, Comput. Mater. Sci. **21**, 291 (2001).
[50] M. Boero, M. Parrinello, K. Terakura, T. Ikeshoji, and C. C. Liew, Phys. Rev. Lett. **90**, 226403/1 (2003).

[51] A. Wallqvist, G. Martyna, and B. J. Berne, J. Phys. Chem. **92**, 1721 (1988); C. Nicolas, A. Boutin, B. Levy, and D. Borgis, J. Chem. Phys. **118**, 9689 (2003); J. Schnitker, K. Motakabbir, P. J. Rossky, and R. Friesner, Phys. Rev. Lett. **60**, 456 (1988).

[52] D. H. Son, P. Kambhampati, T. W. Kee, and P. F. Barbara, J. Phys. Chem. A **105**, 8269 (2001).

[53] D. M. Bartels, K. Takahashi, J. A. Cline, T. W. Marin, and C. D. Jonah, J. Phys. Chem. A **109**, 1299 (2005).